HHS Public Access

Author manuscript

Neuron. Author manuscript; available in PMC 2019 March 07.

Published in final edited form as:

Neuron. 2018 March 07; 97(5): 1023–1031.e7. doi:10.1016/j.neuron.2018.01.031.

TREM2 is a receptor for β-amyloid which mediates microglial function

Yingjun Zhao[1,6], **Xilin Wu**[1,2,6], **Xiaoguang Li**[1,6], **Lu-Lin Jiang**[1,6], **Xun Gui**[3], **Yan Liu**[1,4], **Yu Sun**[1], **Bing Zhu**[1], **Juan C. Piña-Crespo**[1], **Muxian Zhang**[4], **Ningyan Zhang**[3], **Xiaochun Chen**[2], **Guojun Bu**[4,5], **Zhiqiang An**[3], **Timothy Y. Huang**[1], and **Huaxi Xu**[1,4,7,*]

[1]Neuroscience Initiative, Sanford Burnham Prebys Medical Discovery Institute, La Jolla, CA 92037, USA

[2]Department of Neurology, Union Hospital, and Fujian Key Laboratory of Molecular Neurology, Fujian Medical University, Fuzhou, Fujian 350001, China

[3]Texas Therapeutics Institute, The Brown Foundation Institute of Molecular Medicine, University of Texas Health Science Center at Houston, Houston, TX 77030, USA

[4]Fujian Provincial Key Laboratory of Neurodegenerative Disease and Aging Research, Institute of Neuroscience, College of Medicine, Xiamen University, Xiamen, Fujian 361102, China

[5]Department of Neuroscience, Mayo Clinic, Jacksonville, FL 32224, USA

SUMMARY

Mutations in *triggering receptor expressed on myeloid cells 2* (*TREM2*) have been linked to increased Alzheimer's disease (AD) risk. Neurobiological functions of TREM2 as well as its pathophysiological ligands remain elusive. Here we found that TREM2 directly binds to β-amyloid (Aβ) oligomers with nanomolar affinity, whereas AD-associated *TREM2* mutations reduce Aβ binding. TREM2 deficiency impairs Aβ degradation in primary microglial culture and mouse brain. Aβ-induced microglial depolarization, K^+ inward current induction, cytokine expression and secretion, migration, proliferation, apoptosis and morphological changes are dependent on TREM2. In addition, TREM2 interaction with its signaling adaptor DAP12 is enhanced by Aβ, regulating downstream phosphorylation of SYK and GSK3β. Our data

*Correspondence: H.X. (xuh@sbpdiscovery.org).

[6]These authors contributed equally to this work

[7]Lead Contact

AUTHOR CONTRIBUTIONS

Y.Z. and H.X. conceived the study and supervised X.W. and X.L.; X.W. performed a majority of the Aβ binding assays; X.G. and N.Z. performed SPR and BLI assays; Y.Z. and X.L. carried out Aβ phagocytosis/degradation and qRT-PCR assays, and stereotaxic injections; Y.Z. performed cytokine multiplex assays; L.J. performed histological analysis; Y.L., Y.S. and J.P.C. performed electrophysiological analysis; B.Z. performed FRET assays; M.Z., X.C., G.B. and T.Y.H. provided essential discussion; Z.A. supervised X.G.; Y.Z. L.J. and H.X. analyzed data; Y.Z., T.Y.H. and H.X. wrote the manuscript.

DECLARATION OF INTERESTS

The authors declare no competing interests.

demonstrate TREM2 as a microglial Aβ receptor transducing physiological and AD-related pathological effects associated with Aβ.

INTRODUCTION

Alzheimer's disease (AD) is an age-dependent neurodegenerative disorder characterized by senile plaques enriched with β-amyloid (Aβ) peptides, and neurofibrillary tangles comprised of hyperphosphorylated tau (Selkoe and Hardy, 2016). Oligomeric forms of Aβ (oAβ) are believed to trigger a pathological cascade leading to AD (Selkoe and Hardy, 2016). Recent genome-wide association studies have identified numerous genetic loci altered in AD (Harold et al., 2009; Hollingworth et al., 2011; Lambert et al., 2013), which may not impact directly on Aβ generation or tau aggregation. Interestingly, a subset of these genes including *TREM2 (Triggering Receptor Expressed on Myeloid cells 2), CD33, CR1, MS4A, ABCA7* and *EPHA1* are expressed in myeloid cell types and microglia, suggesting that immune cell dysfunction may play a key role in AD pathogenesis (Efthymiou and Goate, 2017). In addition to familial β-amyloid precursor protein (APP), presenilin (PS) 1/2 alleles linked to early AD onset (Vetrivel et al., 2006), variations in ApoE (ε4) and the TREM2 ectodomain (R47H) are currently associated with the highest risk of AD (Guerreiro and Hardy, 2013; Guerreiro et al., 2013; Jonsson et al., 2013). Additional variants of the TREM2 ectodomain (R62H) are also linked to increased AD risk (Jin et al., 2014). TREM2 has been shown to mediate phagocytic clearance of apoptotic cell debris and modulate inflammatory response (Doens and Fernandez, 2014; Jay et al., 2017b; Kleinberger et al., 2014). TREM2 binds to its adaptor, DNAX-activating protein of 12 kDa (DAP12) on the surface of microglia to enact innate immune responses and downstream cellular responses or signaling pathways (Jay et al., 2017b). Despite recent identification of lipids and ApoE as TREM2 ligands (Atagi et al., 2015; Wang et al., 2015; Yeh et al., 2016), biological ligands for TREM2 and their consequent impact on microglial function in AD pathogenesis remains unclear.

RESULTS

TREM2 Binds to Aβ Oligomers

To determine whether TREM2 could function as a receptor for Aβ, we prepared synthetic $Aβ_{1–42}$ monomers and oligomers (Figures S1A and S1B) using protocols previously reported (Kim et al., 2013) and investigated whether the TREM2 ectodomain (TREM2-Fc) could bind to Aβ. TREM2-Fc co-precipitated with oAβ and, to a much lesser extent, with Aβ monomers; minimal binding was observed with TREM1-Fc or Fc controls (Figures 1A, B and S1C). Immobilized TREM2-Fc bound to oAβ with an affinity comparable to previously described Aβ receptor proteins such as CD36-Fc and RAGE-Fc (Figure 1C); with TREM2-Fc exhibiting little binding with Aβ monomers (data not shown). Similarly, immobilized oAβ bound TREM2-Fc with a comparable affinity to CD36-Fc and RAGE-Fc (Figure 1D), with little interaction detected in Fc and TREM1-Fc controls. Bio-Layer Interferometry assays consistently demonstrated high affinity Aβ interactions with TREM2-His (K_D = 12.7 ± 0.5 nM) (Figure 1E); where TREM1-His showed minimal oAβ binding (Figure 1F). We also confirmed Aβ/TREM2 interactions using surface plasmon resonance (SPR) assays (Figure S1D). Interestingly, TREM2 R47H or R62H mutation compromised

TREM2-Fc interactions with oAβ in solid phase binding assays (Figure 1G). In agreement with these results, increased oAβ binding was observed in microglia-derived BV2 cells with stable TREM2 overexpression (Figure 1H), where TREM2 mRNA and protein levels were determined to be elevated to almost 3-fold and 2.5-fold respectively (Figure S1E and F), compared to BV2 controls. Likewise, TREM2 also co-immunoprecipitated with Aβ in BV2 cells incubated with oAβ (Figure S1G). Importantly, an endogenous Aβ/TREM2 complex was co-immunoprecipitated from AD mouse brain lysates (TgCRND8, overexpressesing mutant human β-amyloid precursor protein, APP) (Figure 1I) and human AD brain lysates (Figures 1J and S1H–J). Although we were unable to differentiate binding of Aβ monomers from oligomers in our assays, we anticipate that TREM2 interacts preferentially to oAβ as seen in our *in vitro* binding assays.

TREM2 Regulates Aβ Degradation and Aβ-Induced Depolarization in Microglia

We next determined whether TREM2 could modulate microglial Aβ catabolism. Given that a variety of Aβ surface receptors are redundantly expressed in microglia (Doens and Fernandez, 2014), it was not surprising that TREM2 deletion had little effect on surface binding (Figure S2A) and phagocytic uptake of Aβ in microglia (Figure 2A). However, we found that TREM2-deficient microglia showed significantly reduced Aβ degradation; fluorescent dye FAM-labeled Aβ was largely cleared 2–4 h after internalization in wildtype (WT), but mostly retained in TREM2 knockout (KO) microglia (Figures 2B–D). Although Aβ degradation was inhibited by exposure to the proteasomal inhibitor MG132, only partial effects were observed using a lysosomal/autophagy inhibitor (chloroquine, CQ) (Figures 2C and D). These results were confirmed by ELISA using unlabeled oAβ (Figure S2B). In agreement with partial effects in Aβ turnover with CQ, only a small fraction of Aβ was found in LAMP1-positive compartments (Figure S2C). These results indicate that TREM2 mediates Aβ catabolism largely through proteasomal degradation pathways. Indeed, it is widely accepted that proteasome and lysosome pathways are interconnected through autophagosomes (Kwon and Ciechanover, 2017). How TREM2 is involved in proteasome- and/or lysosome-mediated Aβ degradation warrants further examination. We also determined whether TREM2 deletion affects turnover rates of ligands for other microglial receptors, such as Gas6 which has been previously reported to bind to the MerTK receptor (Chen et al., 1997). We found little or no Gas6 binding to TREM2 (Figure S2D); fluorescent-labeled Gas6 featured slower turnover rates compared to Aβ, where WT and TREM2 KO microglia showed no differences in Gas6 degradation (Figure S2E). Together, these data support a specific role for TREM2/Aβ interactions in Aβ degradation.

Next, we characterized electrophysiological effects of oAβ on microglial membranes in culture. Induction of potassium (K^+) currents by oAβ has been shown to promote microglial membrane depolarization (Franciosi et al., 2006). We observed significant depolarization and associated changes in resting membrane potential (RMP) with oAβ treatment and TREM2 deletion; however, oAβ failed to induce further changes in membrane potential with TREM2 deletion (Figure 2E). Blocking either Kv1.3 or Kir3.1 channels eliminated the effect of TREM2 deficiency on RMP (Figure S2F). The presence of K^+ currents in microglia is an early indicator of microglial activation associated with increased microglial excitability, proliferation, chemotaxis and migration (Boucsein et al., 2000; Lam and Schlichter, 2015).

We then characterized K^+ inward current induction and observed similar changes as seen in membrane potential above (Figures 2F–H). Since TREM2 KO microglia did not show a corresponding decrease in cell capacitance (Figure S2G), the effect of TREM2 deficiency on K^+ inward current was not due to decreased membrane surface area in TREM2 KO microglia. Together, this suggests a role for TREM2 in mediating oAβ-dependent changes in microglial excitability through K^+ inward currents and provides functional evidence for the significant downregulation of K^+ channels such as Kir4.1 (KCNJ10), Kir7.1 (KCNJ13) and Kir 5.1 (KCNJ16) in TREM2 deficient microglia as described previously (Ulland et al., 2017; Wang et al., 2015). Given the central role inwardly rectifying K+ channels play in resting membrane potential and transition from resting to activated states, reduced expression of functional K^+ channels is a key contributing factor to the depolarized RMP observed in TREM2 deficient microglia.

TREM2 Deficiency Alters Aβ-Induced Cytokine Expression/Secretion and Downstream Signaling

Microglia are critical mediators of the inflammatory response in brain. We observed increased expression of proinflammatory cytokines such as *interleukin 6* (*IL-6*) and *macrophage inflammatory protein 1 α* (*MIP-1α*, also known as *CCL3*), and decreased anti-inflammatory *Arg1* expression with oAβ exposure in WT microglia, whereas Aβ-induced effects on cytokine production were abolished in TREM2 KO microglia (Figure 3A). Using multiplex ELISA assays, we next examined cytokine secretion profiles from cultured WT and TREM2 KO microglia in the presence or absence of oAβ. Exposure to oAβ for 24h or 48h resulted in significantly elevated secretion of IL-6, and MIP-1α in WT microglia, with little or no oAβ-induced change observed in TREM2 KO microglia (Figures 3B and C). We did not observe any significant oAβ-induced changes in IL-1α, IL-4, interferon γ (IFN-γ) and tumor necrosis factor α (TNF-α) secretion in WT and TREM2 KO microglia; steady-state levels of these cytokines were also equivalent in WT and TREM2 KO microglia (Figures S3A and S3B).

As our results suggest that TREM2 mediates Aβ-induced microglial response, we next investigated downstream events that potentially drive TREM2-dependent microglial activation. Interestingly, interaction between TREM2 and its obligate adaptor DAP12 was increased in primary microglia with acute Aβ exposure (30–60 min), as indicated by fluorescence resonance energy transfer (FRET) assay (Figure 3D) and TREM2/DAP12 co-immunoprecipitation assays (Figures 3E and S3C). Overexpression of TREM2 increased DAP12 levels (Figure S3D), likely due to stabilizing interactions previously described (Zhong et al., 2015); where TREM2-DAP12 interactions were further enhanced by oAβ treatment (Figure S3E). In addition, brief oAβ exposure induced SYK phosphorylation (a key component of the TREM2/DAP12 signaling pathway) in WT, but not TREM2 KO microglia (Figure 3F). Overexpression of human TREM2 in a BV2 microglial cell line pretreated with mouse TREM2 shRNA dramatically increased GSK3β phosphorylation under steady-state conditions, and further enhanced GSK3β phosphorylation with oAβ treatment; while little change was observed with Aβ treatment in control BV2 cells lacking human TREM2 (Figure S3F). These results indicate that TREM2 is required for downstream signal transduction in response to Aβ stimulation.

TREM2 Deficiency Alters Aβ Degradation, Microglial Migration, Proliferation and Apoptosis in Response to Aβ *in vivo*

We next determined the effects of stereotactic Aβ injection in WT and TREM2 KO mouse brain. At 16 hours post-injection, we found a significant decrease in the number of microglia clustering at FAM-Aβ-enriched regions in TREM2 KO compared to WT, as indicated by IBA1 immunostaining (Figures 4A and B), whereas FAM-Aβ deposition was similar between WT and TREM2 KO brain at this time point (Figure 4C). No microglia clustering was observed in control vehicle-injected WT or TREM2 KO mouse brain (Figure S4). These results suggest that TREM2 deletion attenuates microglial migration in response to acute Aβ injection. We next investigated microglial response to extended Aβ exposure in WT and TREM2 KO mice. We observed decreased hippocampal Aβ clearance in TREM2 KO mice 3 days after oAβ injection into the microglia-enriched lacunosum moleculare layer within the hippocampus where fewer neuronal cell bodies are found (Figures 4D and E). This is in good agreement with recent findings that TREM2 modulation may regulate Aβ pathology (Yuan et al., 2016). Upon stereotactic oAβ injection, we observed an increase in microglial proliferation (PCNA positivity) and caspase-3 activation in WT mice (Figures 4F and G), indicative of Aβ-induced-microgliosis and apoptotic cell death which may occur concurrently (Askew et al., 2017). Interestingly, TREM2 deletion largely abolished Aβ-induced microglial proliferation (Figure 4F) and apoptosis (Figure 4G). Additionally, microglial process length, previously shown to be associated with microglial activation (Zhong et al., 2017), was found to be significantly reduced in Aβ-injected WT brain, but not in TREM2 KO brain (Figure 4H).

Together, our results provide evidence that TREM2/Aβ interactions can mediate downstream TREM2/DAP12 signaling pathways, thereby triggering microglial Aβ degradation and microglia depolarization, activation and consequent cytokine expression/release. TREM2 also drives microglial activation and migration to sites of Aβ enrichment *in vivo*, indicating that TREM2 is an Aβ sensor which mediates Aβ clearance, and Aβ-dependent microglia activation and cytokine release.

DISCUSSION

Although a role for TREM2 in AD pathogenesis has been recently proposed, opposing effects on Aβ plaque deposition are observed with TREM2 deletion in differing AD models (Jay et al., 2015; Wang et al., 2015), which may be attributed to differences in genetic backgrounds, and/or additional effects derived from APP/PS1 overexpression (Cavanaugh et al., 2014; Lee and Han, 2013). Interestingly, recent work in APP/PS1 AD mouse model indicates that TREM2 deletion can reduce Aβ plaque load at early stages of AD onset, yet exacerbates Aβ deposition at late stages of onset (Jay et al., 2017a). As the involvement of TREM2 in Aβ-associated pathogenesis is likely complex, a definitive model of how TREM2 contributes mechanistically to Aβ pathology and AD pathogenesis has yet to be established. Our work provides pioneering evidence that TREM2 directly interacts with Aβ and regulates Aβ degradation, and demonstrates a novel role for TREM2 as a microglial Aβ receptor capable of transducing various microglial responses to Aβ.

Changes in MIP-1α in response to Aβ are particularly interesting: in addition to playing a key role in inflammation, MIP-1α has been shown to promote microglial activation and migration (Wang et al., 2008). The absence of Aβ-induced MIP-1α induction in TREM2 KO microglia may contribute to reduced microglial clustering at Aβ deposits. Interestingly, TREM2 deficiency has been recently shown to attenuate microglial migration towards injured neurons (Mazaheri et al., 2017). Together, our findings demonstrate that TREM2 plays an important role in mediating microglial migration in response to pathological stimuli.

Our observation that AD-associated R47H and R62H mutations compromise interactions between Aβ and TREM2 provides a plausible mechanism for TREM2 and its disease-prone genetic variants in AD pathogenesis. Our findings are in good agreement with recent structural analysis predicting that AD-associated TREM2 mutations might compromise a potential TREM2 ligand-binding interface (Kober et al., 2016). Our previous work, and evidence from other groups have identified ApoE and lipids as TREM2 ligands (Atagi et al., 2015; Wang et al., 2015; Yeh et al., 2016). Since ApoE is the most potent genetic risk factor associated with late-onset AD (Kanekiyo et al., 2014), together with evidence of dysfunctional lipid metabolism in AD (Di Paolo and Kim, 2011; Walter and van Echten-Deckert, 2013), it will be interesting to determine the interplay between ApoE, lipids, and Aβ in TREM2 signaling in future studies.

Although our results present evidence that Aβ-induced microglial response is in part mediated through TREM2 function, there remains a possibility that Aβ-derived effects may be also derived through parallel pathways, or through indirect microglial changes with TREM2 deletion. Although TREM2 is not a component of ion channels, our results indicate that TREM2 deletion itself could induce changes in membrane inward current and membrane potential. Thus, the possibility remains that although TREM2/Aβ interactions likely drive some microglia-modulating effects with Aβ exposure, there may also be secondary changes with perturbation resulting from TREM2 deletion that may also modulate Aβ-dependent signaling and microglial function. A detailed analysis of the potential significance of alternative pathways and secondary changes is indeed interesting, and warrants further investigation. As current strategies targeting Aβ generation and use of Aβ antibody clearance have seen little success, modulation of microglial clearance through receptors such as TREM2 may be a favorable alternative for future pharmacological development.

STAR METHODS

EXPERIMENTAL MODEL AND SUBJECT DETAILS

Mouse Models—TREM2 knockout (KO) mouse strain was kindly provided by Dr. John Fryer at Mayo Clinic. Wild type (WT) C57BL/6N mouse strain was from The Jackson Laboratory. Both KO and WT animals were maintained as homozygous lines. TgCRND8 mice in a hybrid C3H/He-C57BL/6 background were provided by Dr. Xiongwei Zhu (Case Western Reserve University) and Dr. Peter St. George-Hyslop (University of Toronto) (Chishti et al., 2001). Postnatal day 2–3 WT and TREM2 KO mice were used for primary microglial cultures. Since hormonal effects are negligible at this stage, mixed primary

microglial cultures were taken from both males and females. Only 3–4 month old male WT and TREM2 KO mice were used for Aβ injection analysis. Only 9–10 month old male TgCRND8 mice were used for analysis. Animal procedures did not include additional drug or treatment regimen other than that described. Mouse lines were housed with littermates with free access to food and water with a 12 hour light/day cycle. All animal procedures, including husbandry were performed under the guidelines of the Institutional Animal Care and Use Committee at Sanford Burnham Prebys Medical Discovery Institute.

Cell Culture Models—BV2 cells (originating from female mice) and human embryonic kidney (HEK) 293T cells (sex information is not available) were obtained from ATCC and cultured in DMEM containing 10% FBS. Cell lines were authenticated by the providers. BV2 cells stably expressing human TREM2 were generated using lentiviral vectors comprising a PGK promoter upstream of a human TREM2 cDNA-IRES2-EGFP module (GeneCopoeia).

Human Samples—Human brain tissues were obtained from Brain Bank Resources offered by the University of Miami or University of California, San Diego. The use of human brain samples in this study is exempt from Institutional Review Board review (exemption #4) according to the criteria set forth by United States Department of Health and Human Services. No statistical methods were used for sample size estimation. Human brain samples were processed and analyzed with institutional permission in accordance with California and National Institutes of Health guidelines. All samples were subjected to IP with IgG and TREM2 antibody. Information with respect to previous procedures for human subjects was not disclosed with the tissue samples used. No data were excluded in the experiments described. Detailed information for human samples (gender, age and disease stage) can be found in Table S1.

CONTACT FOR REAGENT AND RESOURCE SHARING

Further information and requests for reagents may be directed to and will be fulfilled by the corresponding author, Huaxi Xu (xuh@sbpdiscovery.org).

METHOD DETAILS

Cell culture and generation of stable cell lines—Primary microglial cultures were prepared as described previously (Atagi et al., 2015). Briefly, brains were removed from WT or TREM2 KO mice at postnatal day 2–3. After removal of the meninges, brains were treated with a Papain Dissociation System (Worthington Biochemical Corporation) according to manufacturer's specifications. Mixed glial cells were plated in flasks coated with poly-D-lysine and grown in DMEM containing 10% FBS (VWR Life Science Seradigm). 25 ng/mL GM-CSF (R&D Systems) was added into the cultures after 5 days and removed before harvesting. Microglial cells were harvested twice by shaking (200 rpm, 60 min) 10–14 days after plating and subjected to various treatments within 24 h of harvest.

BV2 and human embryonic kidney (HEK) 293T cells were from ATCC and cultured in DMEM containing 10% FBS. BV2 cells stably expressing human TREM2 were generated using lentiviral vectors comprising a PGK promoter and human TREM2 cDNA-IRES2-

EGFP module (GeneCopoeia). Lentiviral particles (Lv-TREM2) were packaged through the viral core at Sanford Burnham Prebys Medical Discovery Institute. BV2 cells were transduced with Lv-TREM2 or control lentivirus (Lv-control) and single EGFP-positive cells were sorted by flow cytometry using a high speed cell sorter (BD Biosciences FACSAriaIIu). Single clonal cell lines were expanded and characterized for expression. To knockdown endogenous mouse TREM2, lentiviruses expressing shRNA specifically targeting mouse *TREM2* mRNA (5' – CCAGUCCUUGAGGGUGUCAUGUACU – 3') were transduced to BV2 stable cell lines. No mycoplasma contamination was detected in cell lines used in this study.

Aβ preparation—Aβ monomers and oligomers were prepared as described previously with slight modification (Kim et al., 2013). Unlabeled or biotin-labeled synthetic human $Aβ_{1–42}$ peptides (Anaspec) were dissolved in hydroxyfluroisopropanol (HFIP) and subsequently dried using a SpeedVac system (Thermo Fisher Scientific). Monomers were prepared by dissolving the lyophilized Aβ in dimethyl sulfoxide (DMSO) at 2.2 mM, sonicated for 10 min and diluted in PBS to 100 μM. Aβ oligomers were prepared in DMSO/PBS and oligomerized by incubation at room temperature (RT) for 48 h. Monomers in the oligomer preparation were removed using Amicon Ultra Centrifugal Filters (Millipore) (10 kDa molecular weight cut-off). Samples from each step were collected and analyzed by immunoblotting. No difference in oligomerization between normal and biotin-Aβ was observed.

Carboxyfluorescein (FAM) -Aβ aggregates were prepared as described previously (Kleinberger et al., 2014). Briefly, FAM-$Aβ_{1–42}$ peptides (Anaspec) were dissolved in trifluoroacetic acid, lyophilized using a SpeedVac, and dissolved in DMSO/ PBS to 100 μM at 37°C overni ght.

Immunoprecipitation assay and Aβ ELISA—In cell-free binding assays, 0.5 μg human IgG1 Fc, TREM2-Fc or TREM1-Fc (R&D Systems) was incubated with 0.25 μg unlabeled or biotin-labeled Aβ monomer or oligomers in TBS buffer (25 mM Tris-HCl pH 7.6, 150 mM sodium chloride) containing 0.05% Tween-20 (TBST) and Dynabeads protein G (Thermo Fisher Scientific) at 4°C for 2 h. Beads were then washed with TBST fo ur times and boiled in SDS-PAGE loading buffer (BioPioneer) containing 62.6 mM Tris-HCl (pH 6.8), 2% SDS, 0.01% bromophenol blue, 10% glycerol and 0.5M dithiothreitol and subjected to immunoblot analysis. No difference in TREM2 binding between unlabeled and biotin-labeled Aβ was observed (data not shown). These experiments were repeated 5 times. Randomization procedures are not applicable to these experiments. Data were collected and analyzed in a double-blind fashion. No statistical methods were used for sample size estimation. No data were excluded.

Endogenous Aβ/TREM2 interactions were determined using brain tissues from TgCRND8 APP transgenic mice (9-month old) or from human AD patients. Tissues or cells were lysed in TBS containing 5 mM ethylenediaminetetraacetic acid (EDTA), 1% Nonidet P40 substitute (T-DET O-9) with protease inhibitors (Roche), and incubated with TREM2 antibodies (rat anti-TREM2 antibody for TgCRND8 samples, MABN755, Millipore; rabbit anti-human TREM2 antibody for human brain samples, 91068, Cell Signaling Technology) /

Dynabeads protein G at 4°C overnight. Beads were wa shed four times in TBST and boiled in SDS-PAGE loading buffer or a buffer containing 0.2% SDS and 0.1% Tween-20. Samples were analyzed by immunoblotting or enzyme-linked immunosorbent assay (ELISA) using a human $A\beta_{1–42}$ ELISA kit (Thermo Fisher Scientific). Human Aβ was undetectable in our IP-ELISA assays from wildtype (WT) mouse brain (data not shown), confirming specific detection of human Aβ using this IP-ELISA detection method. Randomization procedures are not applicable to these experiments. Data were collected from 3 experiments (5 samples from TgCRND8 mice, 6 samples from human AD patients) and analyzed in a double-blind fashion. No statistical methods were used for sample size estimation. No data were excluded.

Solid phase binding assay—Human IgG1 Fc, TREM2-Fc, TREM1-Fc, CD36-Fc, RAGE-Fc proteins (R&D systems), or TREM2-Fc proteins (WT and mutants) purified in-house were coated onto Nunc MaxiSorp 96-well plates (Thermo Fisher Scientific) at 0.2 μg/well in TBS at 4°C overnight. After block ing in 5% non-fat milk in TBS for 2h at room temperature, biotin-Aβ oligomers equivalent to 6.25, 12.5, 25, 50, 100, or 200 nM Aβ monomers were added to the plates at 4°C overnight. Plates were washed with TBS containi ng 0.05% Tween-20 (TBST, Sigma) four times and incubated with streptavidin-HRP (1:5000, Thermo Fisher Scientific) for 30 min at RT. Plates were then washed with TBST three times, developed in TMB solution (Thermo Fisher Scientific), and absorbance at 450 nM was measured using a Synergy H1 microplate reader (BioTek).

Similar to the above, 0.1 μg biotin-Aβ oligomers were immobilized on plates and incubated with 6.25, 12.5, 25, 50, 100, or 200 nM human IgG1 Fc, TREM2-Fc, TREM1-Fc, CD36-Fc or RAGE-Fc. Bound Fc proteins were detected by anti-human IgG-HRP (1:5000, Thermo Fisher Scientifc) and developed in TMB solution as described.

These experiments were repeated 3 times. Randomization procedures are not applicable to these experiments. Data were collected and analyzed in a double-blind fashion. No statistical methods were used for sample size estimation. No data were excluded.

Generation of TREM2-Fc proteins—cDNA comprising the human *TREM2* extracellular region (1–174 amino acids) was cloned into pFUSE-hIgG1-Fc (Invivogen). R47H and R62H TREM2-Fc mutant vectors were generated using the QuikChange II Site-Directed Mutagenesis kit (Agilent Technologies), following the manufacturer's recommendations. Fc vectors were transfected into HEK293T cells with Lipojet (Version 2, SignaGen Laboratories). TREM2-Fc proteins were collected in serum-free DMEM and purified with protein A/G beads (Thermo Fisher Scientific), followed by elution in 0.2M glycine pH 2.8, neutralization and dialysis. Protein yields were subsequently determined by BCA protein assay.

Immunoblotting—Prepared samples were subjected to gel electrophoresis (4–20% SDS-PAGE, Bio-Rad laboratories) and probed using relevant antibodies. The following primary antibodies were used for immunoblot: mouse monoclonal antibody against $A\beta_{1–12}$ (B436) (Huang et al., 2016), rabbit monoclonal antibody against human TREM2 (clone D814C, 91068, Cell Signaling Technology) (Ma et al., 2016), goat anti-human TREM2 antibody

(AF1828, R&D Systems), sheep anti-mouse TREM2 antibody (AF1729, R&D Systems), mouse monoclonal c-Myc tag antibody (13–2500, Thermo Fisher Scientific), mouse monoclonal antibody for Gas6 (clone A-9, sc-376087, Santa Cruz Biotechnology), rabbit monoclonal antibody against DAP12 (Clone D7G1X, 12492, Cell Signaling Technology) rabbit monoclonal antibody for phospho-SYK (clone F.724.5, MA5-14918, Thermo Fisher Scientific), rabbit monoclonal antibody for SYK (Clone D3Z1E, 13198, Cell Signaling Technology), and mouse monoclonal antibody against β-actin (Clone AC-74, A2228, Sigma). To reduce IgG signals in immunoprecipitates, TrueBlot secondary antibodies against mouse, goat, or rabbit IgG were used (Rockland). These experiments were repeated 3–5 times (see details in the Figure Legends). Randomization procedures are not applicable to these experiments. Data were collected and analyzed in a double-blind fashion. No statistical methods were used for sample size estimation. No data were excluded.

Affinity measurement with Bio-Layer Interferometry (BLI) and Surface Plasmon Resonance (SPR)—BLI was performed using the Octet system 8-channel Red96 system (Pall Life Sciences). SA biosensors and kinetics buffer were purchased from Pall Life Sciences. Biotin-Aβ oligomers were immobilized onto SA biosensors and incubated with varying concentrations (2.74 nM to 222 nM) of TREM2-His or TREM1-His proteins in solution. The experiments included five steps: (*i*) biotin-Aβ oligomers loading onto SA biosensors (240 s); (*ii*) baseline (10 s); (*iii*) association of TREM2-His or TREM1-His for measurement of K_{on} (120 s); and (i*v*) dissociation of Aβ oligomers for the measurement of K_{dis} (600 s). Baseline and dissociation steps were conducted in 1 × kinetics buffer and background subtraction was used to correct for biosensor drifting. Background wavelength shifts were measured from reference biosensors that were loaded only with biotin-Aβ oligomers. All experiments were performed at 30°C w ith shaking at 1,000 rpm. ForteBio's data analysis software 7.0 was used to fit the data to a 1:1 binding model.

SPR was determined using Biacore T100 instrument (GE Health). TREM2-Fc (20 μg/ml) was captured on the GAH (goat anti-human) IgG immobilized CM5 sensor surface. Binding of a dilution series comprising biotin-Aβ oligomers (16 nM to 1000nM) to TREM2-Fc was analyzed and fitted to the 1:1 binding model using BIAevaluation software.

These experiments were repeated 3 times. Randomization procedures are not applicable to these these assays. No statistical methods were used for sample size estimation. No data were excluded.

Cell surface Aβ binding assay—Cells were incubated with 200 nM biotin-Aβ oligomers or FAM-Aβ aggregates at 4 °C for 2 h. Cells were then washed five times with cold PBS and fixed in 4% PFA without permeabilization. Cell surface bound Aβ was detected using a streptavidin-Alexa Fluor 555 conjugate (1:500, Thermo Fisher Scientific) or directly subjected to confocal imaging. Bound Aβ was analyzed using IMARIS. At least 400 cells for each group were analyzed from 3–5 independent experiments. Randomization procedures are not applicable to these experiments. Data were collected and analyzed in a double-blind fashion. No statistical methods were used for sample size estimation. No data were excluded.

Aβ phagocytosis and degradation assay—To determine the effect of TREM2 deletion on Aβ phagocytosis, primary microglial cultures from WT or TREM2 KO mice were incubated with FAM-Aβ (200 nM) for 30 min, 1 h or 2 h. Following the removal of FAM-Aβ, cells were trypsinized, washed with cold PBS and subjected to flow cytometry analysis using a LSRFortessa X-20 cell analyzer (BD Biosciences). Surface bound FAM-Aβ was quenched by incubation with 0.4% trypan blue in PBS (pH 4.4) for 1 min prior to FACS analysis.

For Aβ degradation, cells were washed three times with DMEM 2 h after FAM-Aβ or unlabeled Aβ oligomers phagocytosis and cultured for an additional 2 or 4 hours (in FAM-Aβ-free media), and analyzed by flow cytometry or ELISA analysis at varying timepoints. Alternatively, cells with FAM-Aβ were fixed in 4% paraformaldehyde (PFA) and visualized using an LSM 710 confocal microscope (ZEISS). FAM-Aβ intensity was analyzed and quantified using IMARIS software (Bitplane). At least 500 cells from each group were analyzed from three independent experiments.

These experiments were repeated 3 times. Randomization procedures are not applicable to these experiments. Data were collected and analyzed in a double-blind fashion. No statistical methods were used for sample size estimation. No data were excluded.

Gas6 degradation assay—Recombinant Gas6 protein (R&D systems) was labeled with Alexa Fluor 488 microscale protein labeling kit following manufacturer's instructions. Primary microglial cultures from WT or TREM2 KO mice were incubated with fluorescent-labeled Gas6 (100 nM) for 2 h. Following the removal of Gas6, cells were washed three times and cultured for an additional 4 or 22 hours and analyzed by flow cytometry using a LSRFortessa X-20 cell analyzer (BD Biosciences). Surface bound fluorescent-labeled Gas6 was quenched by incubation with 0.4% trypan blue in PBS (pH 4.4) for 1 min prior to FACS analysis.

These experiments were repeated 3 times. Randomization procedures are not applicable to this assay. Data were collected and analyzed in a double-blind fashion. No statistical methods were used for sample size estimation. No data were excluded.

Electrophysiology—Treated microglia cells were recorded under voxltage clamp conditions. Patch pipettes with a tip resistance of 5–8 MΩ were pulled from borosilicate glass capillaries (B150-86-10, Sutter) using a laser micropipette puller (P-2000, Sutter). Patch pipettes were filled with an intracellular solution of the following composition (in mM): K-gluconate 123, KCl 6, $CaCl_2$ 1, $MgCl_2$ 4.6, EGTA 10, HEPES 10, Na_2-GTP 0.4, Na_2-ATP 4.0, pH 7.24 adjusted with KOH. The extracellular recording solution comprised of Hank's balanced salt solution (HBSS, 14025, Gibco) supplemented with 10 mM HEPES, 5 mM glucose and adjusted to pH 7.4 with NaOH. A series of hyperpolarizing voltage steps from −60 mV to −160 mV (Δ=10 mV) were applied using a computer-controlled patch-clamp amplifier (Axopatch 200B, Molecular Devices) connected to an analog to digital converter (Digidata 1322A, Molecular Devices). To block Kv1.3 or Kir 3.1 channel, cells were incubated for 1 h with 400 pM Margatoxin or 100 nM Tertiapin (Alomone, Israel), respectively. Whole-cell capacitance was measured under voltage clamp configuration by

applying a 5 mV pulse from a membrane potential of −60 mV. Electrophysiological recordings were taken from 4 independent microglial cultures. Randomization procedures are not applicable to this assay. Data were collected and analyzed in a double-blind fashion. No statistical methods were used for sample size estimation. No data were excluded.

Quantitative real-time (qRT) - PCR—Total RNA was purified from cells using the RNeasy Universal Mini Kit (Qiagen) following manufacturer's specifications. Purified RNA was then transcribed to cDNA using the SuperScript III Reverse Transcriptase system (Thermo Fisher Scientific), and subjected to qPCR reactions using the FastStart Universal SYBR Green Master (Rox) system (Roche) with primers targeting mouse *GAPDH, IL-6, MIP-1α* and *Arg1*. Primer sequences are as follows:

TREM2,	forward 5'-AGGGCCCATGCCAGCGTGTGGT-3',
	Reverse 5'-CCAGAGATCTCCAGCATC-3';
GAPDH,	forward 5'-CCCTTCATTGACCTCAACTA-3',
	reverse 5'-CCTTCTCCATGGTGGTGAA-3';
IL-6,	forward 5′-TAGTCCTTCCTACCCCAATTTCC-3′,
	reverse 5′-TTGGTCCTTAGCCACTCCTTC-3′.
MIP-1α,	forward 5′-CCCAGCCAGGTGTCATTTTCC-3′,
	reverse 5′-GCATTCAGTTCCAGGTCAGTG-3′;
Arg1,	forward 5′-CACAGTCTGGCAGTTGGAAGC-3′,
	reverse 5′-CTTTGGCAGATATGCAGGGAG-3′.

These experiments were repeated 3 times. Randomization procedures are not applicable to this assay. Data were collected and analyzed in a double-blind fashion. No statistical methods were used for sample size estimation. No data were excluded.

Multiplex Cytokine ELISA assay—Primary microglial cells were treated with 0, 0.2 μM or 1 μM Aβ oligomers for 24h or 48h. Conditioned medium was collected and analyzed using a mouse cytokine multiplex kit (Quansys), following the manufacturer's recommendations. Cytokine measurements falling under the detection threshold (below lower limits of the standard curve) are not presented. These experiments were repeated 3 times. Randomization procedures are not applicable to this assay. Data were collected and analyzed in a double-blind fashion. No statistical methods were used for sample size estimation. No data were excluded.

Fluorescence resonance energy transfer (FRET) assay—FRET experiments were performed as previously described (Zhu et al., 2017). Briefly, average of fluorescence intensities of the donor before and after bleaching was calculated from the measurement of 6 cells in three independent experiments per group. Randomization procedures are not applicable to this assay. Data were collected and analyzed in a double-blind fashion. No statistical methods were used for sample size estimation. No data were excluded. FRET efficiency was calculated by $E_{fret} = 1-(I_a/I_b)$, where I_a and I_b represents the steady-state donor fluorescence with or without the acceptor, respectively.

Stereotaxic injections—Stereotaxic injections were performed as described previously with modifications (Wang et al., 2014; Zhao et al., 2015). Random WT or TREM2 KO mice (4–5 month old) were anesthetized using 2% isoflurane, and Aβ oligomers (5μg in 2μL vehicle/side) or control vehicle (PBS containing 4% DMSO) were injected bilaterally into the hippocampus at the following coordinates: anterior posterior, −2.2 mm; medial lateral, ± 1.5 mm; dorsal ventral, −1.8 mm using an automated stereotaxic injection apparatus (Model 940, KOPF). Mice were sacrificed and analyzed 3 days after injection.

For migration analysis, FAM-Aβ aggregates or control vehicle were injected unilaterally into the hippocampus and cortex at the following coordinates: anterior posterior, −2 mm; medial lateral, ± 1.5 mm; dorsal ventral, −2 and −1 mm (Mazaheri et al., 2017). Mice were sacrificed and analyzed 16 hours after injection.

Immunohistological analysis—Mice were anesthetized with 4% isoflurane and intracardially perfused with PBS. Brain tissues were harvested and fixed in 4% paraformaldehyde at 4 °C for 24 h. Tissues were washed in PBS and cryoprotected in PBS containing 30% sucrose. Tissues were embedded in OCT containing 30% sucrose (at 1:1 v/v) and free-floating coronal brain cryostat sections (25 μm) were collected. Data were collected and analyzed in a double-blind fashion. For Aβ detection, brain sections were immunostained with MOAB-2 (M-1586-100, Biosensis) followed by an anti-mouse HRP secondary antibody, and developed using a DAB substrate (Vector Laboratories). Sections were counter-stained with hematoxylin, and images were acquired and analyzed using a ScanScope AT2 system (Leica Biosystems).

For detection of IBA1, cleaved caspase 3, and PCNA, brain slices were stained using antibodies as follows: Goat anti-IBA1 (1:400, ab5076, Abcam), rabbit anti-cleaved-caspase 3 (1:200, 9664, Cell Signaling Technology), rabbit anti-PCNA (1:400, 13110, Cell signaling Technology). Alexa Fluor 488, 568 or 647 secondary antibodies were used, DAPI counterstains were applied to the sections, and image z-stacks were acquired from multiple sections (up to 9) from each animal using a Zeiss confocal microscope (LSM 710). Cleaved-caspase-3/IBA1 and PCNA/IBA1 positive cells were manually counted. Process length of IBA1 positive cells were analyzed using IMARIS.

QUANTIFICATION AND STATISTICAL ANALYSIS

Statistical details of the experiments, including sample sizes, definition of center, dispersion, and statistical tests can be found in the figures and accompanying figure legends. Results are displayed as mean ± s.d. Samples sizes are comparable to those described previously in similar studies (Cisse et al., 2011; Kim et al., 2013), although statistical methods were not used to predetermine sample sizes in all the assays. Standard deviations were calculated to determine whether the data met assumptions of the statistical approach. No data or subjects were excluded in this study. Statistical analyses were performed with GraphPad Prism software (version 7). Differences were assessed by paired or unpaired t tests, or one-way or two-way ANOVA where appropriate. P values < 0.05 were considered as statistically significant. Specified description of n numbers in Figure 1:

(B) *n*=5 independent experiments, (C) *n* = 3 independent experiments, (D) *n* = 3 independent experiments. (G) *n* = 3 independent experiments, (H) *n* = 5 independent experiments, (I) *n* = 5 mouse samples, (J) *n* = 6 for human AD samples.

Specified description of *n* numbers in Figure 2:

(A, B, and D) *n*= 3 independent microglial cultures from 15 animals for each genotype, (E) WT-control, *n* = 7; WT-Aβ, *n* = 8; KO-control, *n* = 8; KO-Aβ, *n* = 7 cells, (G) TREM2 KO, *n* = 18; WT, *n* = 9 cells, (H) *n* = 5 cells for each group. For (E, G and H) cells were from 4 independent microglial cultures from 18 animals for each genotype.

Specified description of *n* numbers in Figure 3:

(A–C) *n* = 3 independent microglial cultures from 15 animals for each genotype, (D) *n* = 6 cells per group from three experiments, (E) *n* = 5 independent microglial cultures from 28 animals, (F) *n* = 3 independent microglial cultures from 20 animals for each genotype.

Specified description of *n* numbers in Figure 4:

(B and C) WT, *n* = 8, KO, *n* = 9 animals, (E) WT, *n* = 9, KO, *n* = 8 animals, (F) WT-control, *n* = 12, WT-Aβ, *n* = 11, KO-control, *n* = 10, KO-Aβ, *n* = 11 animals, (G) WT-control, *n* = 8, WT-Aβ, *n* = 11, KO-control, *n* = 10, KO-Aβ, *n* = 11 animals, (H) WT-control, *n* = 9, WT-Aβ, *n* = 12, KO-control, *n* = 11, KO-Aβ, *n* = 12 animals.

DATA AND SOFTWARE AVAILABILITY

Data supporting findings from this study is available from the corresponding author upon reasonable request.

Supplementary Material

Refer to Web version on PubMed Central for supplementary material.

Acknowledgments

We thank John D. Fryer at Mayo Clinic for providing TREM2 KO mice, and Xiongwei Zhu at Case Western Reserve University and Peter St. George-Hyslop at University of Toronto for providing TgCRND8 mice. This work was supported by grants from National Institute of Health (R21 AG048519, R01 AG021173, R01 AG038710, R01 AG044420, R01 NS046673, and RF1 AG056114 to H.X,; and RF1 AG056130 to G.B. and H.X.); by grants from the National Natural Science Foundation of China (U1505227 to G.B., U1405222 to H.X., 81771163 to H.X.); by the Tanz Family Fund (to H.X.) and Cure Alzheimer's Fund (to G.B and H.X.); and by the Welch Foundation Grant No. AU-0042-20030616 (to Z.A.).

References

Askew K, Li K, Olmos-Alonso A, Garcia-Moreno F, Liang Y, Richardson P, Tipton T, Chapman MA, Riecken K, Beccari S, et al. Coupled Proliferation and Apoptosis Maintain the Rapid Turnover of Microglia in the Adult Brain. Cell Rep. 2017; 18:391–405. [PubMed: 28076784]

Atagi Y, Liu CC, Painter MM, Chen XF, Verbeeck C, Zheng H, Li X, Rademakers R, Kang SS, Xu H, et al. Apolipoprotein E Is a Ligand for Triggering Receptor Expressed on Myeloid Cells 2 (TREM2). J Biol Chem. 2015; 290:26043–26050. [PubMed: 26374899]

Boucsein C, Kettenmann H, Nolte C. Electrophysiological properties of microglial cells in normal and pathologic rat brain slices. Eur J Neurosci. 2000; 12:2049–2058. [PubMed: 10886344]

Cavanaugh SE, Pippin JJ, Barnard ND. Animal models of Alzheimer disease: historical pitfalls and a path forward. ALTEX. 2014; 31:279–302. [PubMed: 24793844]

Chen J, Carey K, Godowski PJ. Identification of Gas6 as a ligand for Mer, a neural cell adhesion molecule related receptor tyrosine kinase implicated in cellular transformation. Oncogene. 1997; 14:2033–2039. [PubMed: 9160883]

Chishti MA, Yang DS, Janus C, Phinney AL, Horne P, Pearson J, Strome R, Zuker N, Loukides J, French J, et al. Early-onset amyloid deposition and cognitive deficits in transgenic mice expressing a double mutant form of amyloid precursor protein 695. J Biol Chem. 2001; 276:21562–21570. [PubMed: 11279122]

Cisse M, Halabisky B, Harris J, Devidze N, Dubal DB, Sun B, Orr A, Lotz G, Kim DH, Hamto P, et al. Reversing EphB2 depletion rescues cognitive functions in Alzheimer model. Nature. 2011; 469:47–52. [PubMed: 21113149]

Di Paolo G, Kim TW. Linking lipids to Alzheimer's disease: cholesterol and beyond. Nat Rev Neurosci. 2011; 12:284–296. [PubMed: 21448224]

Doens D, Fernandez PL. Microglia receptors and their implications in the response to amyloid beta for Alzheimer's disease pathogenesis. J Neuroinflammation. 2014; 11:48. [PubMed: 24625061]

Efthymiou AG, Goate AM. Late onset Alzheimer's disease genetics implicates microglial pathways in disease risk. Mol Neurodegener. 2017; 12:43. [PubMed: 28549481]

Franciosi S, Ryu JK, Choi HB, Radov L, Kim SU, McLarnon JG. Broad-spectrum effects of 4-aminopyridine to modulate amyloid beta1–42-induced cell signaling and functional responses in human microglia. J Neurosci. 2006; 26:11652–11664. [PubMed: 17093087]

Guerreiro R, Hardy J. TREM2 and neurodegenerative disease. N Engl J Med. 2013; 369:1569–1570. [PubMed: 24143816]

Guerreiro R, Wojtas A, Bras J, Carrasquillo M, Rogaeva E, Majounie E, Cruchaga C, Sassi C, Kauwe JS, Younkin S, et al. TREM2 variants in Alzheimer's disease. N Engl J Med. 2013; 368:117–127. [PubMed: 23150934]

Harold D, Abraham R, Hollingworth P, Sims R, Gerrish A, Hamshere ML, Pahwa JS, Moskvina V, Dowzell K, Williams A, et al. Genome-wide association study identifies variants at CLU and PICALM associated with Alzheimer's disease. Nat Genet. 2009; 41:1088–1093. [PubMed: 19734902]

Hollingworth P, Harold D, Sims R, Gerrish A, Lambert JC, Carrasquillo MM, Abraham R, Hamshere ML, Pahwa JS, Moskvina V, et al. Common variants at ABCA7, MS4A6A/MS4A4E, EPHA1, CD33 and CD2AP are associated with Alzheimer's disease. Nat Genet. 2011; 43:429–435. [PubMed: 21460840]

Huang TY, Zhao Y, Li X, Wang X, Tseng IC, Thompson R, Tu S, Willnow TE, Zhang YW, Xu H. SNX27 and SORLA Interact to Reduce Amyloidogenic Subcellular Distribution and Processing of Amyloid Precursor Protein. J Neurosci. 2016; 36:7996–8011. [PubMed: 27466343]

Jay TR, Hirsch AM, Broihier ML, Miller CM, Neilson LE, Ransohoff RM, Lamb BT, Landreth GE. Disease Progression-Dependent Effects of TREM2 Deficiency in a Mouse Model of Alzheimer's Disease. J Neurosci. 2017a; 37:637–647. [PubMed: 28100745]

Jay TR, Miller CM, Cheng PJ, Graham LC, Bemiller S, Broihier ML, Xu G, Margevicius D, Karlo JC, Sousa GL, et al. TREM2 deficiency eliminates TREM2+ inflammatory macrophages and ameliorates pathology in Alzheimer's disease mouse models. J Exp Med. 2015; 212:287–295. [PubMed: 25732305]

Jay TR, von Saucken VE, Landreth GE. TREM2 in Neurodegenerative Diseases. Mol Neurodegener. 2017b; 12:56. [PubMed: 28768545]

Jin SC, Benitez BA, Karch CM, Cooper B, Skorupa T, Carrell D, Norton JB, Hsu S, Harari O, Cai Y, et al. Coding variants in TREM2 increase risk for Alzheimer's disease. Hum Mol Genet. 2014; 23:5838–5846. [PubMed: 24899047]

Jonsson T, Stefansson H, Steinberg S, Jonsdottir I, Jonsson PV, Snaedal J, Bjornsson S, Huttenlocher J, Levey AI, Lah JJ, et al. Variant of TREM2 associated with the risk of Alzheimer's disease. N Engl J Med. 2013; 368:107–116. [PubMed: 23150908]

Kanekiyo T, Xu H, Bu G. ApoE and Abeta in Alzheimer's disease: accidental encounters or partners? Neuron. 2014; 81:740–754. [PubMed: 24559670]

Kim T, Vidal GS, Djurisic M, William CM, Birnbaum ME, Garcia KC, Hyman BT, Shatz CJ. Human LilrB2 is a beta-amyloid receptor and its murine homolog PirB regulates synaptic plasticity in an Alzheimer's model. Science. 2013; 341:1399–1404. [PubMed: 24052308]

Kleinberger G, Yamanishi Y, Suarez-Calvet M, Czirr E, Lohmann E, Cuyvers E, Struyfs H, Pettkus N, Wenninger-Weinzierl A, Mazaheri F, et al. TREM2 mutations implicated in neurodegeneration impair cell surface transport and phagocytosis. Sci Transl Med. 2014; 6:243ra286.

Kober DL, Alexander-Brett JM, Karch CM, Cruchaga C, Colonna M, Holtzman MJ, Brett TJ. Neurodegenerative disease mutations in TREM2 reveal a functional surface and distinct loss-of-function mechanisms. Elife. 2016; 5

Kwon YT, Ciechanover A. The Ubiquitin Code in the Ubiquitin-Proteasome System and Autophagy. Trends Biochem Sci. 2017; 42:873–886. [PubMed: 28947091]

Lam D, Schlichter LC. Expression and contributions of the Kir2.1 inward-rectifier K(+) channel to proliferation, migration and chemotaxis of microglia in unstimulated and anti-inflammatory states. Front Cell Neurosci. 2015; 9:185. [PubMed: 26029054]

Lambert JC, Ibrahim-Verbaas CA, Harold D, Naj AC, Sims R, Bellenguez C, DeStafano AL, Bis JC, Beecham GW, Grenier-Boley B, et al. Meta-analysis of 74,046 individuals identifies 11 new susceptibility loci for Alzheimer's disease. Nature genetics. 2013; 45:1452–1458. [PubMed: 24162737]

Lee JE, Han PL. An update of animal models of Alzheimer disease with a reevaluation of plaque depositions. Exp Neurobiol. 2013; 22:84–95. [PubMed: 23833557]

Ma L, Allen M, Sakae N, Ertekin-Taner N, Graff-Radford NR, Dickson DW, Younkin SG, Sevlever D. Expression and processing analyses of wild type and p.R47H TREM2 variant in Alzheimer's disease brains. Mol Neurodegener. 2016; 11:72. [PubMed: 27887626]

Mazaheri F, Snaidero N, Kleinberger G, Madore C, Daria A, Werner G, Krasemann S, Capell A, Trumbach D, Wurst W, et al. TREM2 deficiency impairs chemotaxis and microglial responses to neuronal injury. EMBO Rep. 2017; 18:1186–1198. [PubMed: 28483841]

Selkoe DJ, Hardy J. The amyloid hypothesis of Alzheimer's disease at 25 years. EMBO Mol Med. 2016; 8:595–608. [PubMed: 27025652]

Ulland TK, Song WM, Huang SC, Ulrich JD, Sergushichev A, Beatty WL, Loboda AA, Zhou Y, Cairns NJ, Kambal A, et al. TREM2 Maintains Microglial Metabolic Fitness in Alzheimer's Disease. Cell. 2017; 170:649–663. e613. [PubMed: 28802038]

Vetrivel KS, Zhang YW, Xu H, Thinakaran G. Pathological and physiological functions of presenilins. Mol Neurodegener. 2006; 1:4. [PubMed: 16930451]

Walter J, van Echten-Deckert G. Cross-talk of membrane lipids and Alzheimer-related proteins. Mol Neurodegener. 2013; 8:34. [PubMed: 24148205]

Wang HK, Park UJ, Kim SY, Lee JH, Kim SU, Gwag BJ, Lee YB. Free radical production in CA1 neurons induces MIP-1alpha expression, microglia recruitment, and delayed neuronal death after transient forebrain ischemia. J Neurosci. 2008; 28:1721–1727. [PubMed: 18272692]

Wang X, Huang T, Zhao Y, Zheng Q, Thompson, Robert C, Bu G, Zhang Y-w, Hong W, Xu H. Sorting Nexin 27 Regulates Aβ Production through Modulating γ-Secretase Activity. Cell Reports. 2014; 9:1023–1033. [PubMed: 25437557]

Wang Y, Cella M, Mallinson K, Ulrich JD, Young KL, Robinette ML, Gilfillan S, Krishnan GM, Sudhakar S, Zinselmeyer BH, et al. TREM2 lipid sensing sustains the microglial response in an Alzheimer's disease model. Cell. 2015; 160:1061–1071. [PubMed: 25728668]

Yeh FL, Wang Y, Tom I, Gonzalez LC, Sheng M. TREM2 Binds to Apolipoproteins, Including APOE and CLU/APOJ, and Thereby Facilitates Uptake of Amyloid-Beta by Microglia. Neuron. 2016; 91:328–340. [PubMed: 27477018]

Yuan P, Condello C, Keene CD, Wang Y, Bird TD, Paul SM, Luo W, Colonna M, Baddeley D, Grutzendler J. TREM2 Haplodeficiency in Mice and Humans Impairs the Microglia Barrier Function Leading to Decreased Amyloid Compaction and Severe Axonal Dystrophy. Neuron. 2016; 90:724–739. [PubMed: 27196974]

Zhao Y, Tseng IC, Heyser CJ, Rockenstein E, Mante M, Adame A, Zheng Q, Huang T, Wang X, Arslan PE, et al. Appoptosin-Mediated Caspase Cleavage of Tau Contributes to Progressive Supranuclear Palsy Pathogenesis. Neuron. 2015; 87:963–975. [PubMed: 26335643]

Zhong L, Chen XF, Wang T, Wang Z, Liao C, Wang Z, Huang R, Wang D, Li X, Wu L, et al. Soluble TREM2 induces inflammatory responses and enhances microglial survival. J Exp Med. 2017; 214:597–607. [PubMed: 28209725]

Zhong L, Chen XF, Zhang ZL, Wang Z, Shi XZ, Xu K, Zhang YW, Xu H, Bu G. DAP12 Stabilizes the C-terminal Fragment of the Triggering Receptor Expressed on Myeloid Cells-2 (TREM2) and Protects against LPS-induced Pro-inflammatory Response. J Biol Chem. 2015; 290:15866–15877. [PubMed: 25957402]

Zhu B, Jiang L, Huang T, Zhao Y, Liu T, Zhong Y, Li X, Campos A, Pomeroy K, Masliah E, et al. ER-associated degradation regulates Alzheimer's amyloid pathology and memory function by modulating gamma-secretase activity. Nat Commun. 2017; 8(1472)

Highlights

- TREM2 binds Aβ and mediates Aβ degradation and activation in microglia
- TREM2 deletion impairs Aβ-induced microglial signaling
- TREM2 mediates microglial cytokine release, migration and clearance of Aβ deposits
- Aβ/TREM2 interaction may contribute to pathogenesis by modulating microglial function

In Brief

Genetic variations in TREM2 confer AD risk, but AD-related ligands for TREM2 are poorly characterized. Zhao et al. demonstrate that TREM2 is a microglial receptor for Aβ and transduces Aβ-induced downstream signaling, providing insight into microglial pathogenicity in AD.

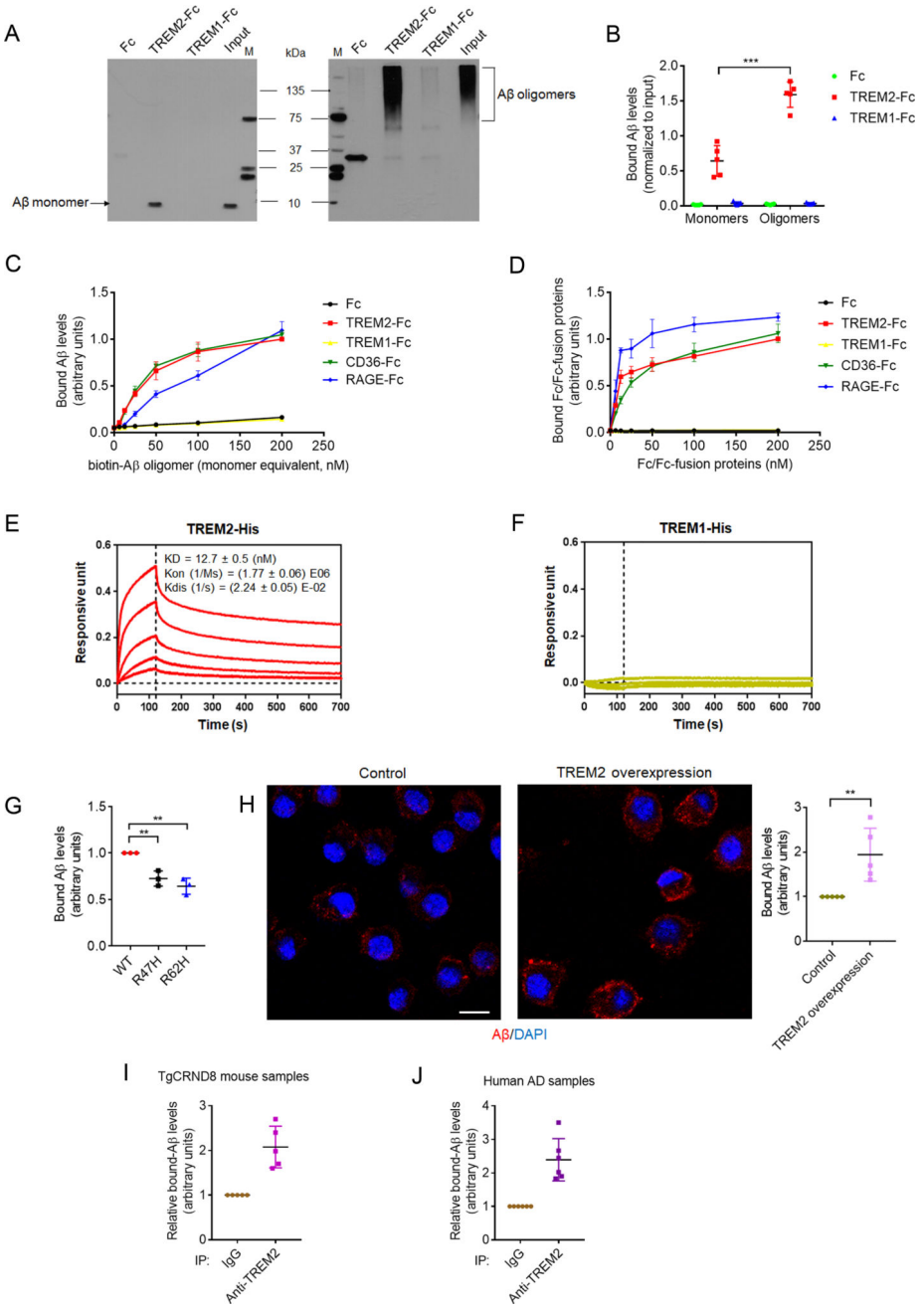

Figure 1. TREM2 binds to Aβ

(A and B) The binding of $A\beta_{1–42}$ monomers or oligomers with Fc, TREM2-Fc or TREM1-Fc. All values were normalized to input. M: marker. n=5 independent experiments, ***P<. 001 by unpaired t-test.

(C) Levels of biotin-o$A\beta_{1–42}$ bound to immobilized Fc/Fc-fusion proteins were normalized to maximal Aβ/TREM2-Fc interactions. n = 3 independent experiments.

(D) Levels of Fc/Fc-fusion proteins bound to immobilized biotin-o$A\beta_{1–42}$ were normalized to maximal TREM2-Fc/Aβ binding. n = 3 independent experiments.

(E and F) Bio-Layer interferometry binding kinetics of TREM2-His (E) or TREM1-His (F) incubated with immobilized biotin-oA$\beta_{1–42}$ (curves correspond to His-tagged proteins with the following concentrations: 222.2nM (top), 74.1nM, 24.7nM, 8.23nM and 2.74nM (bottom); in E and F).

(G) Maximal levels of biotin-oA$\beta_{1–42}$ bound to immobilized wild type (WT) TREM2-Fc, R47H or R62H mutants (normalized to WT). $n = 3$ independent experiments, $^{**}P < 0.01$, one-way ANOVA followed by Dunnett's *post hoc* test.

(H) Representative images of biotin-oA$\beta_{1–42}$ (red) bound to BV2 cells overexpressing TREM2 or BV2 control (DAPI, blue; scale bar = 10 μm). $n = 5$ independent experiments, $^{**}P < 0.01$, unpaired *t*-test.

(I and J) Levels of A$\beta_{1–42}$ co-precipitated with TREM2 in lysates from APP transgenic TgCRND8 mice (I) or human AD brains (J) were determined by ELISA. Bound Aβ was normalized to the IgG control from each sample ($n = 5$ for TgCRND8, $n = 6$ for human AD). All values represent mean ± s.d. See also Figure S1 and Table S1.

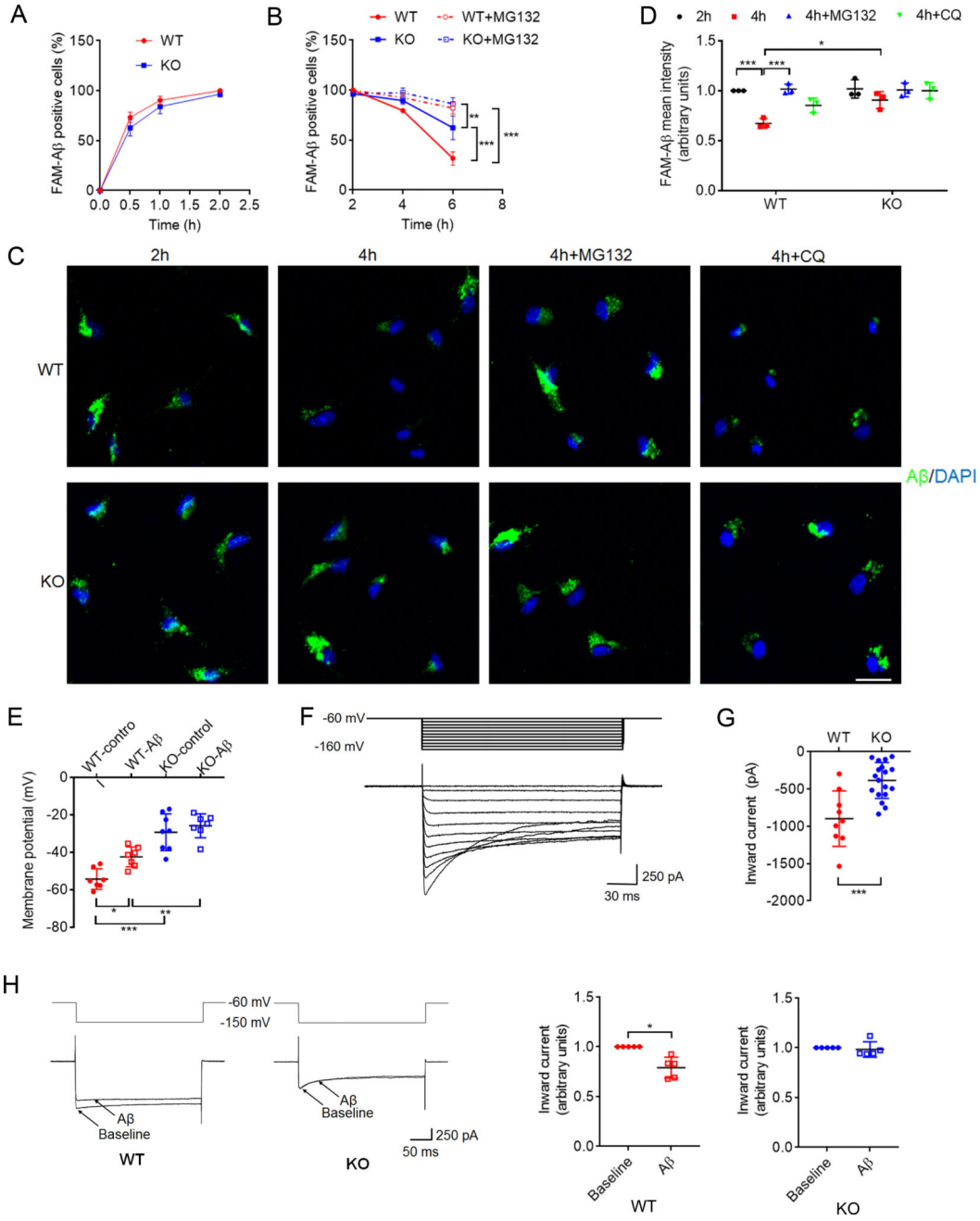

Figure 2. TREM2 deficiency modulates microglia-mediated Aβ degradation, and Aβ-induced depolarization

(A–D) TREM2 deficiency attenuates microglia-mediated Aβ degradation. Cultured microglia from WT or TREM2 KO mice were incubated with 200 nM FAM-$A\beta_{1-42}$ aggregates at 37°C for as the time indicated in (A), and washed/re-incubated in Aβ-free media with or without MG132 (B–D) or chloroquine (CQ) (C and D). FAM-Aβ in WT or TREM2 KO microglia at different time points was determined by flow cytometry (A and B), or confocal microscopy (C). All values were normalized to WT FAM-Aβ levels 2h after uptake. Quantification of FAM-Aβ fluorescence is shown in (D). Scale bar=20 μm. n= 3

independent measurements, $*P < 0.05$, $**P < 0.01$, $***P < 0.001$, two-way ANOVA followed by Tukey *post hoc* test.

(E) Resting membrane potential in WT and TREM2 KO microglia with or without 6h exposure to oA$\beta_{1–42}$ (5 μM). WT-control, $n = 7$; WT-Aβ, $n = 8$; KO-control, $n = 8$; KO-Aβ, $n = 7$. $*P < 0.05$, $**P < 0.01$, $***P < 0.001$, two-way ANOVA followed by Tukey's *post hoc* test.

(F) Representative inward currents obtained from primary microglia.

(G) TREM2 KO microglia showed significantly reduced peak inward currents ($n = 18$ cells) when compared to WT ($n = 9$ cells). $***P < 0.001$, unpaired *t*-test.

(H) A$\beta_{1–42}$ oligomers (10 min) reduce current amplitude in WT but not in TREM2 KO microglia. At −150 mV, current amplitude was significantly reduced in WT but not in TREM2 KO microglia. All values were normalized to baseline for each cell. $n = 5$ cells for each group, $*P < 0.05$, by paired *t*-test. Electrophysiological recordings were taken from 4 independent microglial cultures. All values represent mean ± s.d. See also Figure S2.

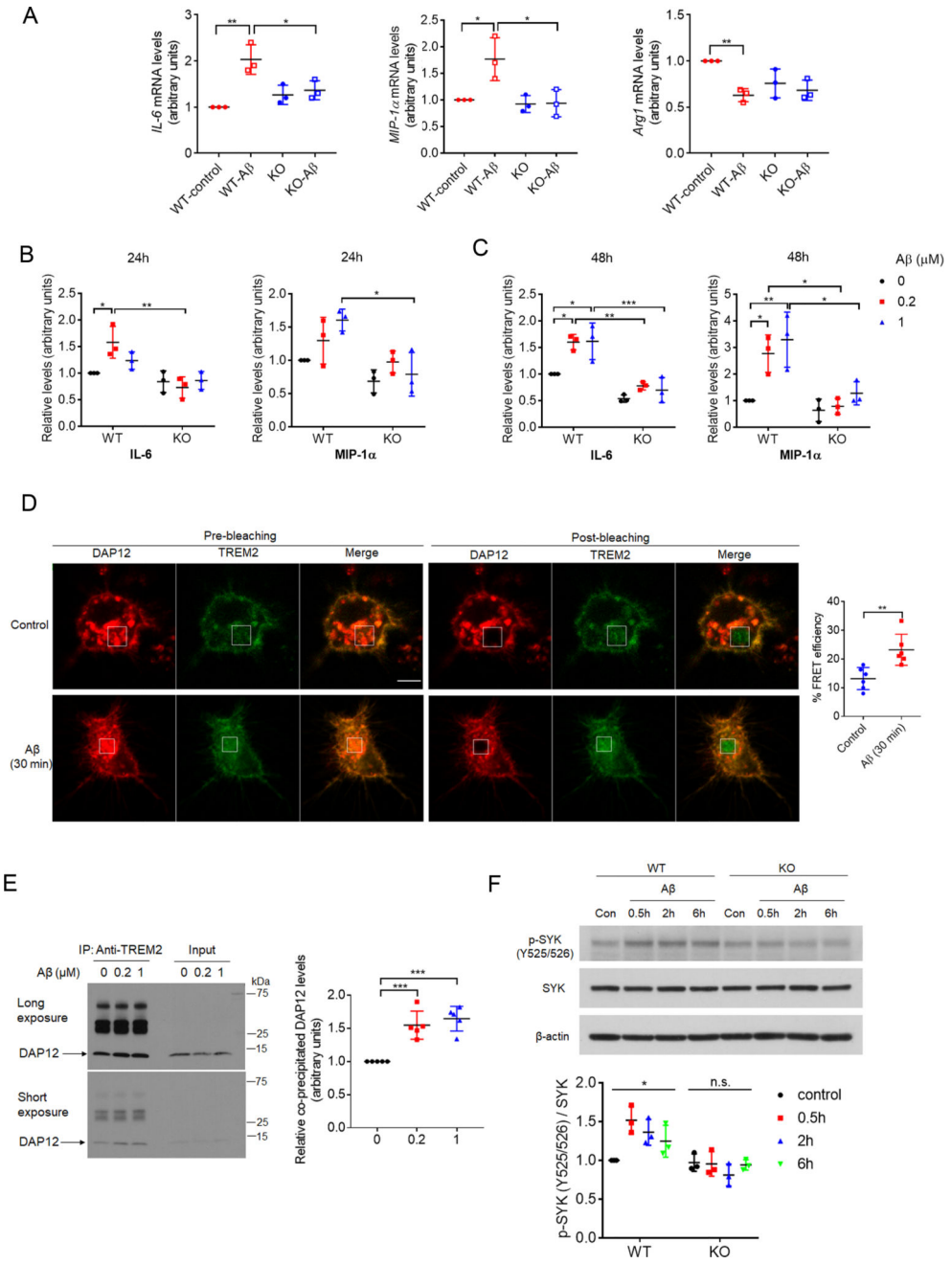

Figure 3. TREM2 deficiency alters microglia cytokine expression/secretion and downstream signaling in response to Aβ

(A) *IL-6, MIP-1α*, or *Arg1* expression was determined by qRT-PCR in WT or TREM2 KO microglia in the presence or absence of 1 μM Aβ. $n = 3$ independent experiments, $*P < 0.05$, $**P < 0.01$, by two-way ANOVA followed by Tukey's *post hoc* test.

(B and C) Cytokines levels in conditioned media from WT or TREM2 KO microglial cultures treated with oA$\beta_{1–42}$ for 24h (B) or 48h (C) were quantified by ELISA. All values were normalized to WT-Aβ (0 μM) levels for each time point. $n = 3$ independent experiments. $*P < 0.05$, $**P < 0.01$, $***P < 0.001$, two-way ANOVA followed by Tukey's *post hoc* test.

(D) BV2 cells overexpressing TREM2-GFP and DAP12-mCherry were treated with or without (1 μM) for 30 min, and interactions between TREM2-GFP and DAP12-mCherry were determined by FRET analysis. White rectangles indicate bleached regions. Scale bar = 10 μm. $n = 6$ cells per group. $^{**}P < 0.01$, unpaired *t*-test.

(E) Levels of endogenous DAP12 co-precipitated with TREM2 in primary microglia treated with oA$\beta_{1–42}$ were determined by Western-blot. $n = 5$ independent experiments. $^{***}P < 0.001$, one-way ANOVA followed by Dunnett's *post hoc* test.

(F) Levels of tyrosine-phosphorylated (Y525/526) and total SYK in WT or TREM2 KO microglia treated with oA$\beta_{1–42}$ (1 μM) were determined by Western blot. $n=3$ independent experiments. $^{*}P<0.05$; n.s., no significance; one-way ANOVA. All values represent mean ± s.d. See also Figure S3.

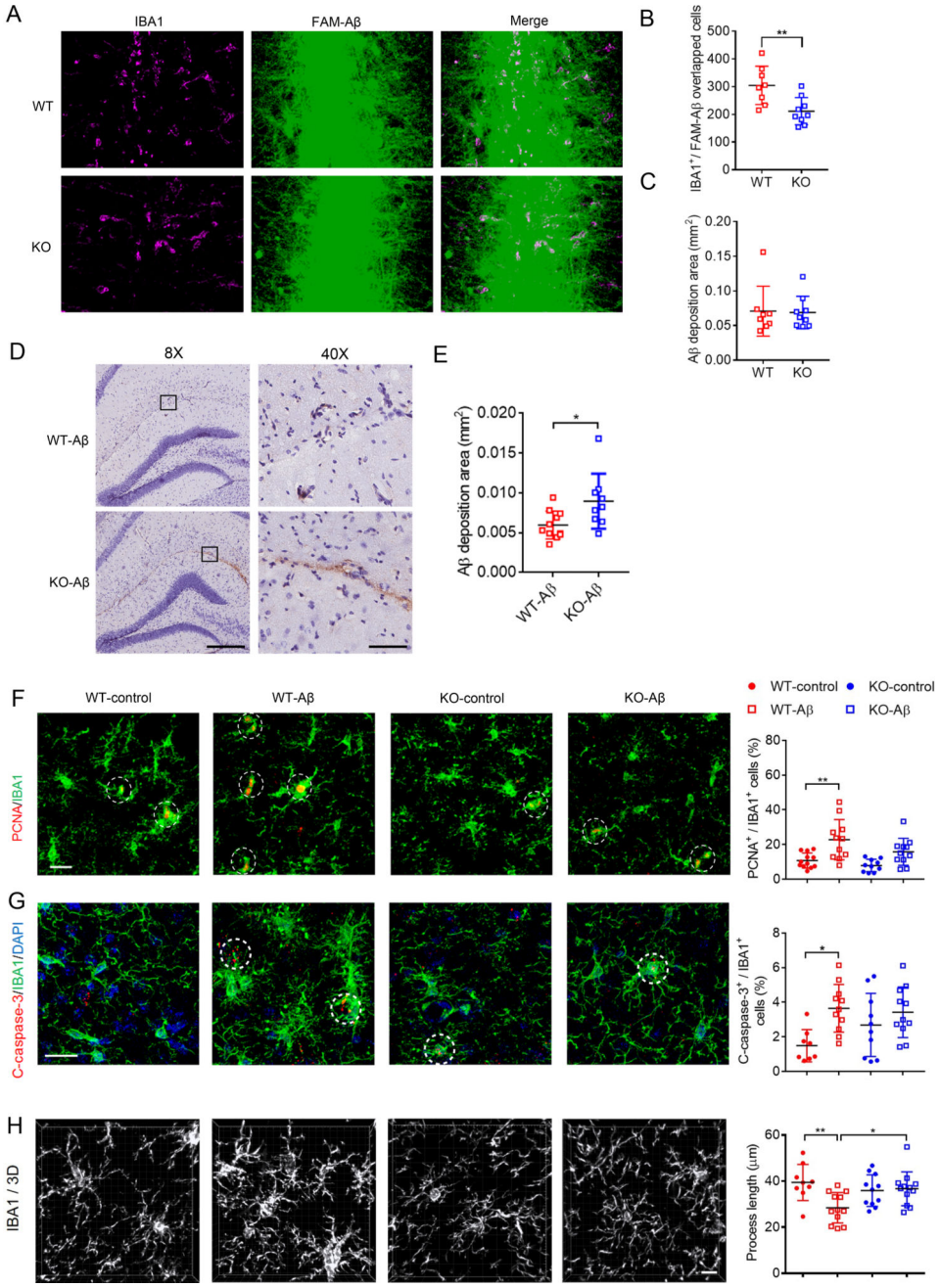

Figure 4. Microglial migration, Aβ degradation and downstream effects on microglial proliferation and apoptosis are altered in TREM2 KO mice

(A–C) Analysis of WT or TREM2 KO brain at 16 hours after FAM-Aβ injection. $n = 8$ for WT, $n = 9$ for KO mice.

(A) Representative images of Aβ injected regions. Scale bar = 20 μm.

(B)Quantified average values for total Aβ/IBA1 positive (IBA1$^+$) cells. $^{**}P < 0.01$ by nonparametric t-test.

(C) Quantified Aβ deposition area.

(D and E) Aβ staining (MOAB-2) in WT or TREM2 KO mouse hippocampus 3 days after oAβ_{1-42} injection (scale bar = 300 μm for 8X magnification, scale bar = 60 μm for 40× magnification in D). $n = 9$ for WT, $n = 8$ for KO mice, $^{*}P < 0.05$ by nonparametric *t*-test. (F and G) Immunostaining of PCNA (red) (F), cleaved-caspase-3 (C-caspase-3, red) (G), IBA1 microglial markers (green) and DAPI (blue) in the hippocampus of WT or TREM2 KO mice with control vehicle or oAβ injection as indicated. PCNA or c-caspase-3 positive microglial cells are indicated by white circles. Adjacent graphs represent quantified overlapping IBA1/PCNA (F) or IBA1/C-caspase-3 (G) stained cells from 8–12 mice per group. Scale bar = 20 μm. $^{*}P < 0.05$, $^{**}P < 0.01$, two-way ANOVA followed by Tukey's *post hoc* test.

(H) Reconstructed 3D microscopy images of IBA1-stained (white) microglia. Average process length per microglia was quantified and shown in the adjacent graph. $n = 9$–12 mice/group. Scale bar = 10 μm $^{***}P < 0.001$, two-way ANOVA followed by Tukey's *post hoc* test. All graphs represent mean ± s.d. See also Figure S4.

KEY RESOURCES TABLE

REAGENT or RESOURCE	SOURCE	IDENTIFIER
Antibodies		
Mouse anti-$A\beta_{1-12}$ (B436)	(Huang et al., 2016)	N/A
Rabbit anti-human TREM2	Cell Signaling Technology	Cat# 91068 RRID:AB_2721119
Goat anti-human TREM2	R&D Systems	Cat# AF1828 RRID:AB_2208689
Sheep anti-mouse TREM2	R&D Systems	Cat# AF1729 RRID:AB_354956)
Mouse anti-Myc	Thermo Fisher Scientific	Cat# 13-2500 RRID:AB_2533008
Mouse anti-Gas6	Santa Cruz Biotechnology	Cat# sc-376087 RRID:AB_10989223
Rabbit anti-phospho-SYK	Thermo Fisher Scientific	Cat# MA5-14918 RRID:AB_10989513
Rabbit anti-SYK	Cell Signaling Technology	Cat# 13198 RRID:AB_2687924
Rabbit anti-DAP12	Cell Signaling Technology	Cat# 12492 RRID:AB_2721120
Mouse anti-β-actin	Sigma	Cat# A2228 RRID:AB_476697
Mouse anti-LAMP1	Santa Cruz Biotechnology	Cat# sc-20011 RRID:AB_626853
Rabbit anti-phospho-GSK3β	Cell Signaling Technology	Cat# 5558 RRID:AB_10013750
Rabbit anti-GSK3β	Cell Signaling Technology	Cat# 12456 RRID:AB_2636978
Rabbit anti-PCNA	Cell Signaling Technology	Cat# 13110 RRID:AB_2636979
Rabbit anti-cleaved-caspase 3	Cell Signaling Technology	Cat# 9664 RRID:AB_2070042
Goat anti-IBA1	Abcam	Cat# ab5076 RRID:AB_2224402
Anti-Aβ antibody MOAB-2	Biosensis	Cat# M-1586-100 RRID:AB_2492497
Biological Samples	For patient information, see Table S1	N/A
Chemicals, Peptides, and Recombinant Proteins		
MG132	EMD Millipore	Cat# 474790
Chloroquine	Cell Signaling Technology	Cat# 14774
Margatoxin	Alomone Labs	Cat# STM-325
Tertiapin	Alomone Labs	Cat# STT-250
$A\beta_{1-42}$ peptides	Anaspec	Cat# AS-20276
Biotin-$A\beta_{1-42}$ peptides	Anaspec	Cat# AS-23523
FAM-$A\beta_{1-42}$ peptides	Anaspec	Cat# AS-23525
Recombinant human IgG1 Fc	R&D Systems	Cat# 110-HG
Recombinant human TREM2-Fc protein	R&D Systems	Cat# 1828-T2
Recombinant human TREM1-Fc protein	R&D Systems	Cat# 1278-TR
Recombinant human CD36-Fc protein	R&D Systems	Cat# 1955-CD
Recombinant human RAGE-Fc protein	R&D Systems	Cat# 1145-RG
Recombinant human Gas6 protein	R&D Systems	Cat# 885-GSB
Recombinant human MerTK-Fc protein	R&D Systems	Cat# 891-MR
Recombinant human TREM2-His protein	Sino Biological	Cat# 11084-H08H
Recombinant human TREM1-His protein	Sino Biological	Cat# 10511-H08H

REAGENT or RESOURCE	SOURCE	IDENTIFIER
Critical Commercial Assays		
Human $A\beta_{1-42}$ ELISA kit	Thermo Fisher Scientific	Cat# KHB3441
Dynabeads protein G	Thermo Fisher Scientific	Cat# 10004D
QuikChange II Site-Directed Mutagenesis kit	Agilent Technologies	Cat# 200523
Lipojet	SignaGen Laboratories	Cat# SL100468
Experimental Models: Cell Lines		
BV2	KCB	Cat# KCB 200770YJ RRID:CVCL_0182
BV2 overexpressing TREM2	This paper	N/A
HEK-293T	ATCC	Cat# CRL-3216 RRID:CVCL_0063
Experimental Models: Organisms/Strains		
C57BL/6N	Jackson Laboratories	Cat# 005304 RRID:IMSR_JAX:00 5304
TREM2 KO mouse	John Fryer (Atagi et al., 2015)	Cat# KOMP:VG10093 RRID:IMSR_KOMP: VG10093
TgCRND8 mouse	Peter St. George-Hyslop (Chishti et al., 2001)	N/A
Oligonucleotides		
TREM2 PCR primer, forward (AGGGCCCATGCCAGCGTGTGGT)	Integrated DNA Technologies	N/A
TREM2 PCR primer, reverse (CCAGAGATCTCCAGCATC)	Integrated DNA Technologies	N/A
GAPDH PCR primer, forward (CCCTTCATTGACCTCAACTA)	Integrated DNA Technologies	N/A
GAPDH PCR primer, reverse (CCTTCTCCATGGTGGTGAA)	Integrated DNA Technologies	N/A
IL-6 PCR primer, forward (TAGTCCTTCCTACCCCAATTTCC)	Integrated DNA Technologies	N/A
IL-6 PCR primer, reverse (TTGGTCCTTAGCCACTCCTTC)	Integrated DNA Technologies	N/A
MIP-1α PCR primer, forward (CCCAGCCAGGTGTCATTTTCC)	Integrated DNA Technologies	N/A
MIP-1α PCR primer, reverse (GCATTCAGTTCCAGGTCAGTG)	Integrated DNA Technologies	N/A
Arg1 PCR primer, forward (CACAGTCTGGCAGTTGGAAGC)	Integrated DNA Technologies	N/A
Arg1 PCR primer, reverse (CTTTGGCAGATATGCAGGGAG)	Integrated DNA Technologies	N/A
Recombinant DNA		
Lentiviral pReceiver-Lv228 vector	GeneCopoeia	EX-NEG-Lv228
Lentiviral pReceiver-Lv228-TREM2 vector	GeneCopoeia	EX-S0483-Lv228
pFUSE-hIgG1-Fc vector	InvivoGen	Cat# pfuse-hg1fc1
pFUSE-TREM2-hIgG1-Fc vector	This paper	N/A
pFUSE-TREM2(R47H)-hIgG1-Fc vector	This paper	N/A
pFUSE-TREM2(R62H)-hIgG1-Fc vector	This paper	N/A
pEGFP-TREM2-N1 vector	This paper	N/A

REAGENT or RESOURCE	SOURCE	IDENTIFIER
pmCherry-DAP12-N1 vector	This paper	N/A
Software and Algorithms		
Fiji-Image J	National Inst. Of Health	https://imagej.net/Fiji RRID:SCR_003070
GraphPad Prism 7	GraphPad	https://www.graphpad.com/scientific-software/prism/ RRID:SCR_015807
Octet software	ForteBio	N/A
BIAevaluation software	GE Healthcare	Cat# BR-1005-97 RRID:SCR_015936
IMARIS	Bitplane	http://www.bitplane.com/imaris/imaris RRID:SCR_007370